Irrig Sci (2016) 34:187–200
DOI 10.1007/s00271-016-0496-6

ORIGINAL PAPER

Monitoring scale-specific and temporal variation in electromagnetic conductivity images

Jingyi Huang[1] · Elia Scudiero[2] · Michael Bagtang[3] · Dennis L. Corwin[2] · John Triantafilis[1]

Received: 9 November 2015 / Accepted: 17 February 2016 / Published online: 4 March 2016

Abstract In semiarid and arid landscapes, irrigation sustains agricultural activity but because of increasing demands on water resources there is a need to make gains in efficiency. As such spatial variation of soil properties such as clay and salinity needs to be understood because they strongly influence soil moisture availability. One way is to use electromagnetic induction because apparent soil electrical conductivity (EC_a) is related to volumetric soil moisture (θ), clay and salinity (EC_e). However, depth-specific variation has not been explored. Our aim is to generate electromagnetic conductivity images (EMCIs) by inverting DUALEM-421 EC_a and show how true electrical conductivity (σ) can be correlated with θ, clay, EC_e and bulk density (ρ) on different days post-irrigation (i.e., 1, 4 and 12 days). Two-dimensional multi-resolution analysis (MRA) is used to show how spatio-temporal variation in σ is scale-specific and how soil properties influence σ at different scales. We study this beneath a pivot irrigated alfalfa crop. We found that σ on days 1 and 4 was correlated with θ (Pearson's $r = 0.79$ and 0.61) and clay (0.86 and 0.80) and the dominant scale of variation occurred at 9.3–18.7 m (50.21 % of total variation), >74.7 m (23.18 %) and 4.7–9.3 m (16.29 %). Between 9.3–18.7 and 4.7–9.3 m the variation may be a function of the cutter width (8 m), while >74.7 m may be change in clay and EC_e and gantry spacing (~48 m). The sprinkler spacing (1.2 and 1.6 m) explains short-scale variation at 1.2–2.3 m.

Communicated by A. Furman.

✉ John Triantafilis
j.triantafilis@unsw.edu.au

[1] School of Biological, Earth and Environmental Sciences, UNSW Australia, Sydney, NSW 2052, Australia

[2] USDA-ARS, U.S. Salinity Laboratory, Riverside, CA 92507-4617, USA

[3] Agricultural Waste Solutions/Scott Brothers Dairy, Moreno Valley, CA 92555, USA

Introduction

In semiarid and arid landscapes, irrigation sustains agricultural activity. However, there are increasing demands on water resources due to climate change and population growth (Vörösmarty et al. 2000). There is therefore a need to make gains in irrigation water use efficiency. As such variation of soil properties such as clay and salinity needs to be understood because they strongly influence soil moisture availability. In addition, the spatio-temporal variation in soil moisture needs to be understood (Knox et al. 2012). Obtaining information in real time is problematic because the thermogravimetric method is time-consuming, slow and expensive (Akbar et al. 2005). This is because measurement of bulk density (ρ—g cm^{-3}) is required to estimate volumetric moisture (θ—cm^3 cm^{-3}). To add value to limited θ, electromagnetic (EM) induction instruments that measure the apparent soil electrical conductivity (EC_a—mS m^{-1}) have been used, because EC_a is a function of θ, when salinity, texture and mineralogy are constant (Corwin et al. 2003; Friedman 2005).

One of the first to recognize the potential use of EM to measure differences in θ were Kachanoski et al. (1988), who established a correlation between EM38 EC_a and average θ to a depth of 0.5 m. Kachanoski et al. (1990) confirmed these results, with a caveat that the calibration was applicable in non-saline soil. Sheets and Hendrickx (1995) extended this along a 1950-m transect by establishing a relationship between EM31 EC_a and θ to 1.5 m. Sherlock

and McDonnell (2003) also demonstrated the ability of EM38 EC_a to predict θ to 0.2 m and at different times. Brevik et al. (2006) showed that along a toposequence EM38 EC_a collected at different times could also be used to make a relationship with θ and for different soil types. However, θ varies with depth and there have been few investigations examining the spatio-temporal variation of θ with depth.

One of the reasons is because there hasn't been readily available software to invert EC_a data into calculated true electrical conductivity (σ—mS m^{-1}) at various depths, otherwise known as electromagnetic conductivity images (EMCIs). However, recent research has shown how a single calibration equation can be developed between σ and various soil properties such as clay (Triantafilis and Monteiro Santos 2009), exchangeable sodium percentage (Huang et al. 2014) and salinity (Goff et al. 2014) along transects and even in 3-d (Li et al. 2013; Zare et al. 2015). Most recently, EMCI has been used to map the spatial variation of θ across a field at various depths (Huang et al. 2016a) and spatio-temporal variation in θ (Huang et al. 2016b) along a transect on various days (i.e., 1, 2, 3, 4, 6, 8 and 12) after an irrigation event. However, scale-specific variation in θ and other environmental factors have not been explored. This is important because it has been shown that a number of environmental factors control its spatio-temporal distribution, including topography, vegetation and texture (Gómez-Plaza et al. 2000; Abdu et al. 2008). To better understand the distribution of θ and improve water management, it is important to delineate correlations between various environmental factors and θ. However, environmental factors often vary at different spatial scales (Corwin et al. 2006; Vanwalleghem et al. 2013). Therefore, it is necessary to characterize the scale-specific correlation between θ and controlling factors.

One approach is the use of the wavelet transform (WT) (Mallat 1999) because it has been used to separate variations in soil properties by locations and scales (Lark et al. 2004; Biswas et al. 2008). WT uses a certain type of wavelet and corresponding scaling functions as the basis to decompose a set of data into components described by wavelet coefficients, which are specific to spatial scales and locations (Lark et al. 2003). Particularly, discrete WT (DWT) can separate variations in soil properties at some preselected scales with twofold increments (Percival and Walden 2000). More commonly this is known as multi-resolution analysis (MRA) and it has been used to understand multi-scale variations in depressions and shelves of gilgai (McBratney 1998) and sedimentary sequences (Lark and Webster 1999). It is also useful for identifying scale-specific correlations between soil properties (Lark et al. 2004). The objectives of this study are to generate EMCI by inverting DUALEM-421 EC_a along a 350-m transect and over a 12-day period to: (1) understand the relationship between σ and various properties (e.g., θ, clay, EC_e and ρ); (2) extract scale-specific spatio-temporal variation in σ using two-dimensional MRA; and (3) understand the scale-specific spatio-temporal variation in σ with depth over 12 days and the scale-specific correlation between σ with other soil properties (i.e., θ, clay, EC_e and ρ).

Materials and methods

Study site

The study field is in southern California's Riverside County (Fig. 1). The field is 32 ha and is located on Scott Brothers' Dairy Farm in San Jacinto (lat. 33° 50′ 25.43″ N, long. 117° 00′ 14.93″ W). The predominant land use is for irrigated

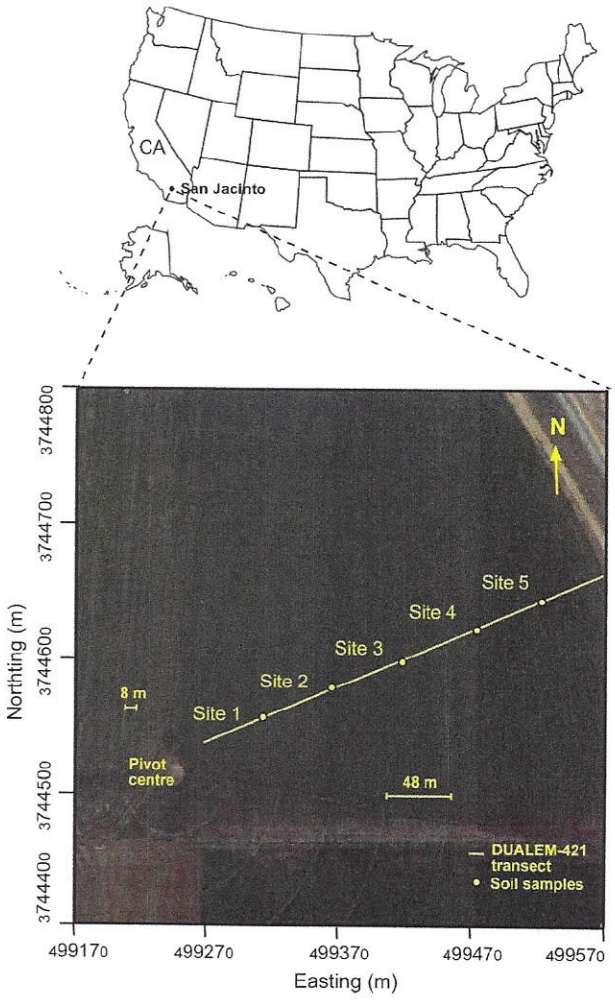

Fig. 1 Location of study area and study transect. *Note* The historical image (06/08/2012) was accessed from Google Earth. The spacing of the tire tracks of the A-frames (48 m) and the alfalfa cutter (8 m) were also marked

alfalfa (*Medicago sativa* L.), which is used for consumption on-farm in a dairy feed lot. The alfalfa is harvested with a cutter which has a width of 8 m, which means the spacing between the tire tracks of the tractor is 8 m (Fig. 1).

The field has been irrigated with dairy lagoon water since March 6, 2008. Corwin et al. (2010) described the average water properties (March 2008 to June 2009) as follows: pH is slightly alkaline (pH = 7.8); slightly (0.7–2.0 dS m^{-1}: Rhoades et al. 1992) saline (EC_{iw} = 1.63 dS m^{-1}) and moderated SAR_w (4.3). The pivot irrigation system consists of irrigation sprinklers which are paired and spaced 1.2 m apart, with the next closest sprinkler 1.6 m away. The length of the entire gantry is 350 m and is supported by A-frames with an average distance of 48 m (Fig. 1).

DUALEM-421 instrument

The DUALEM-421 (DUALM Inc., Milton, ON, Canada) is a single-frequency (9 kHz) and multi-coil array EM induction instrument which operates at low induction numbers and measures apparent electrical conductivity (EC_a, mS m^{-1}). It consists of a transmitting coil (Tx) that has three pairs of receiver coils (Rx) which allows it to measure EC_a at six different depths.

The Tx and one Rx pair have horizontal windings that form a horizontal coplanar array (HCP). The distance between the Tx to the coplanar Rx are 1, 2 and 4 m. The 1mHcon, 2mHcon, and 4mHcon represent EC_a to depths of approximately 0–1.5, 0–3.0 and 0–6.0 m, respectively.

The other coils in each Rx pair have vertical windings and with the Tx forms perpendicular arrays (PRP). The distances between Tx and these Rx are 1.1, 2.1 and 4.1 m, respectively. The respective EC_a measurements are denoted 1mPcon, 2mPcon and 4mPcon with theoretical depth of measurement approximately 0–0.6, 0–1.2 and 0–2.4 m, respectively.

The DUALEM-421S has internal thermometers and a thermal compensation system. According to technical specifications (DUALM Inc., Milton, ON, Canada) the compensation system typically keeps the effect of a 5 °C temperature change on EC_a to a fraction (<2 mS m^{-1}).

Irrigation and EC_a data collection

The study transect is located in the southeastern quadrant of the field. The first and only day of irrigation (40 mm), designated day 1, was carried out on August 28, 2014. Soil EC_a was measured using a DUALEM-421 (Huang et al. 2016b) on this day along the study transect. We also report here on two additional passes made on August 31 (day 4) and September 8 (day 12). To avoid issues requiring temperature correction, the measurements were taken at the same time each day. On each day approximately 600 EC_a were acquired for each of the six DUALEM-421 arrays.

Establishing a calibration between σ and θ

EM4Soil is a software package (EMTOMO 2014) capable of generating electromagnetic conductivity images (EMCIs) that provide estimates of σ from inverted EC_a data. To generate EMCI, a number of parameters can be chosen (Triantafilis and Monteiro Santos 2013), including forward modelling and inversion algorithms and damping factor (λ).

In forward modelling, forward calculations and derivatives consider the cumulative function (CF) or a full-solution (FS) model (Triantafilis et al. 2013). The modelling is conducted using a one-dimensional laterally constrained approach (Auken et al. 2002), where two-dimensional smoothness constraints are imposed. The inversion algorithm, either S1 or S2, are variations of Occam regularization (Sasaki, 1989; 2001). The latter constrains EMCI variation around a reference model and is smoother than S1.

A damping or smoothing factor (λ) is also required. Herein we estimate the true electrical conductivity (σ) using a uniform initial model (σ = 100 mS m^{-1}) and considering the FS and S2 inversion algorithm and $\lambda = 0.3$. We base this on previous work where the optimal parameters were determined to establish a relationship between σ and θ (Huang et al. 2016b).

To compare spatio-temporal variation of σ on the different days, the three EMCI need to be synchronized. We do this because the EC_a data acquired on each day were not measured at the exact same locations. The transects for all intents and purposes were, however, almost near identical as we traversed the same transect every day.

To synchronize the EMCI we used a common 11 × 601 grid. This represents the approximately 600 EC_a data acquired on each day and the vertical spacing of 0.15 m of calculated σ from the EMCI. We achieved synchronization by using a nearest-neighbor algorithm using gstat (Pebesma 2004) with R software. Because the number of σ values of the EMCIs along the transect is approximately 600 (equal to the number of raw EC_a measurements), the synchronization error is small.

Two-dimensional multi-resolution analysis (MRA) of electromagnetic conductivity images (EMCIs)

The two-dimensional multi-resolution analysis (MRA) was conducted using the R Package 'waveslim' (Whitcher 2015). The function 'mra.2d' was selected. It was designed to perform a two-dimensional MRA by performing the one-dimensional pyramid algorithm (Mallat 1989) on the rows and columns of the input matrix (image).

In order to minimize the edge effects for conducting MRA, which is commonly known as cone of influence (Grinsted et al. 2004), we needed to extend the raw EMCI

(11 × 601 grid) to a square array (770 × 770 grid). In this regard we used a symmetry-based approach as described by Lark and Webster (2004). For example, in terms of the EMCI (11 × 601) on day 1, we first flipped the EMCI along its base making a symmetrical image (22 × 601). We then added 34 copies of the symmetrical image to the first symmetrical image and along its base to produce a much larger series of symmetrical images (770 × 601).

Secondly, we flipped the larger series of symmetrical images (770 × 601 grid) to the left and right to produce an extended image (770 × 1803). Lastly, we subset the extended image from the 518th column to the 1287th column and generated a final and square grid (770 × 770), which has extended information at top, bottom, left and right edges and which is continuous at these boundaries. In doing this the aim was to reduce the edge effects of MRA decomposition. We used an identical approach to developing equivalent extended images on days 4 and 12. It is worth noting that by extending the raw EMCIs, we rescale the images in the vertical direction and assume the depth interval is now the same as in the horizontal direction (i.e., 0.58 m) which is supposed to be 0.15 m. The rescaling process was used to accelerate the processing of EMCIs because a conventional way of decomposing images using 1-d MRA will be less efficient (Lark et al., 2003). Because the original EMCI only has 12 layers, which contains much less information in the vertical direction compared to the horizontal direction, we will only study the variations in horizontal direction. The variation in the horizontal direction will not be affected by the rescaling process due to the use of orthonormal wavelet bases (Daubechies, 1992).

Maximal overlap discrete wavelet transform (MODWT) was used to compute the MRA and generate a level J additive decomposition of the input images because the input images (EMCIs) (770 × 770 matrices) do not have the size of 2^n. This will produce a set of images with scales of 0.58 m × 2^J, where 0.58 m is the horizontal sampling interval between two σ readings. J specified the depth of the decomposition and was set to 6. This will decompose the input images into 6 depths, including 6 sets of detailed components in horizontal (LH1, LH2, LH3, LH4, LH5, LH6) and vertical (HL1, HL2, HL3, HL4, HL5, HL6) directions with spatial scales of approximately 1.2–2.3, 2.3–4.7, 4.7–9.3, 9.3–18.7, 18.7–37.3 and 37.3–74.7 m, and one set of smooth component (LL6) at the coarsest resolution (i.e., spatial scale >74.7 m). We chose 6 depths for decomposition because the largest spatial scale (i.e., ~74.7 m) of the coarsest component (i.e., LL6) was less than 1/3 of total length of the transect (i.e., ~350 m). After MRA decomposition, only the coefficient values between the 397th and 407th rows and between the 85th and 685th columns (i.e., an 11 × 601 grid) were used for the following analysis.

Soil sampling and laboratory analysis

To understand the inversion of the DUALEM-421 EC_a and place into some context the wavelet analysis of the calculated σ, 5 soil sample sites were selected (see Fig. 1) approximately an equal distance apart. For reference, site 1 is located at the western end and closest to the center pivot, while site 5 is located farthest away.

At each site soil samples were collected after each EC_a survey and at 0.30 m depths to a maximum of 1.5 m. All samples were sealed in plastic bags. Thermogravimetric moisture content (w—wetness) was determined (g g^{-1}) after a period of 24 h of drying the samples at 105 °C. On the final day 12 undisturbed cores were obtained for bulk density determination (ρ—g cm^{-3}). Volumetric water content (θ) was determined from w and ρ.

The particle size fraction was determined from samples that were air-dried and ground to pass a 2-mm sieve and using the hydrometer method. The electrical conductivity of a saturated soil-paste extract (EC_e—dS m^{-1}) was also determined (U.S. Salinity Laboratory Staff 1954).

Scale-specific contribution of MRA to variance in σ and correlation with various soil properties

To understand scale-specific contribution of MRA components to the total variance in σ, we calculated the standard deviation of the various MRA horizontal (i.e., LH1–LH6) components for days 1, 4 and 12. For each day, we calculated the percentage of the standard deviation of each MRA component (e.g., LH1) over the sum of the standard deviation of all the MRA components in the horizontal direction (i.e., LH1–LH6 and LL6). This approach was used by Biswas et al. (2013) and Huang et al. (2015) to understand the scale-specific contribution of decomposed components to the total variance in the target soil properties in one dimension.

Furthermore, to understand the scale-specific correlation between soil σ with other soil properties, we calculated the Pearson's correlation coefficients (r) between horizontal MRA components with the corresponding measured soil properties, including θ, clay, EC_e and ρ. This will assist in understanding the contribution of different soil properties to the calculated true electrical conductivity (σ) at certain spatial scales and on certain days.

Results and discussion

Distribution of EC_a along transect

Figure 2a shows 1mHcon and 1mPcon collected on the first day. The 1mHcon was slightly larger than 1mPcon. It

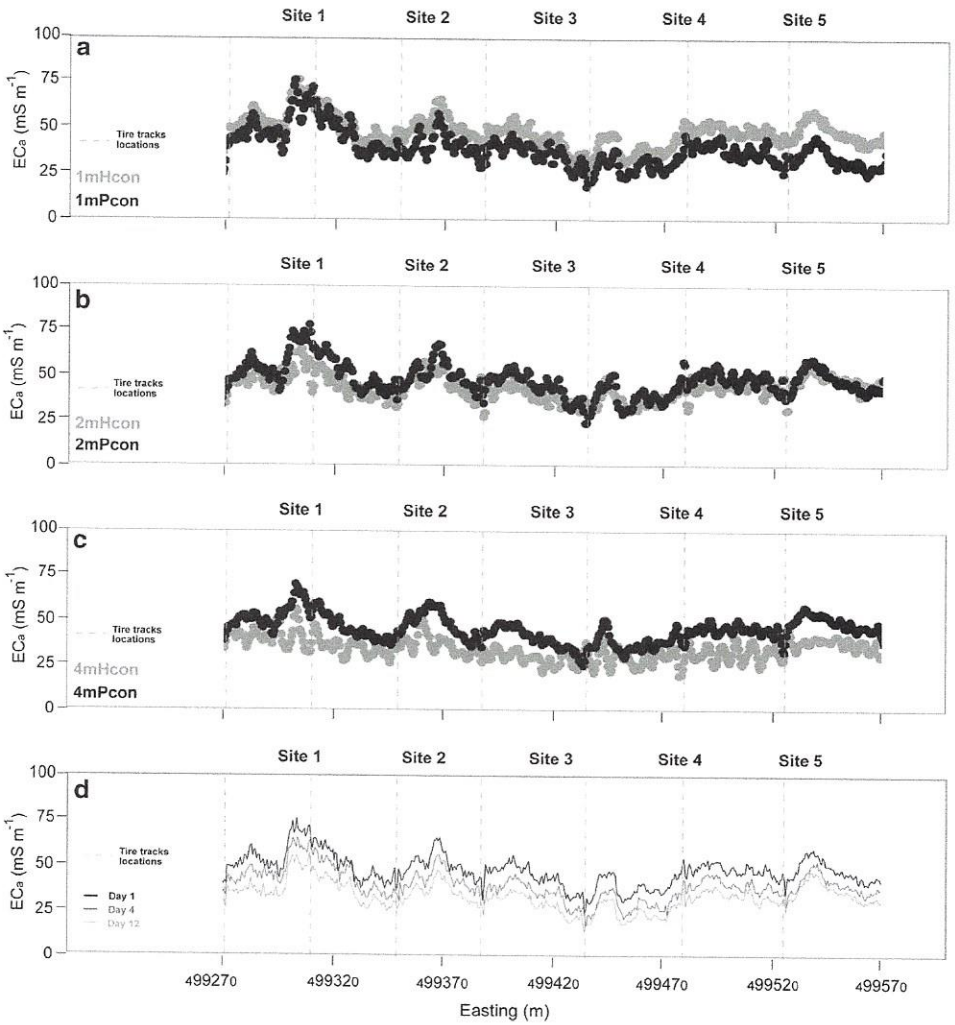

Fig. 2 Distribution of measured apparent soil electrical conductivity (EC_a, mS m^{-1}) by DUALEM-421 along the study transect collected on day 1 and including **a** 1mHcon and 1mPcon, **b** 2mHcon and 2mPcon, **c** 4mHcon and 4mPcon and **d** 1mHcon collected on days 1, 4 and 12

Table 1 Summary statistics of measured apparent electrical conductivity (EC_a, mS m^{-1}) measured by 1-m horizontal coplanar array (1mHcon) of DUALEM-421 on various days after irrigation

Day	Modes	Num.	Min	Mean	Median	Max	Range	Std. Dev.	CV	Skewness
1	1mHcon	524	24.7	47.9	47.5	77.3	52.6	8.3	17.2	0.5
4	1mHcon	527	17.6	40.2	39.7	66.6	49.0	8.0	20.0	0.4
12	1mHcon	601	13.3	33.1	33.1	57	43.7	6.9	21.0	0.3

is worth noting distinct EC_a lows coincide with the wheel tracks and are attributed to soil compaction. Figure 2b shows the 2mHcon and 2mPcon. The EC_a patterns were similar. Figure 2c shows the 4mHcon and 4mPcon. It is evident that EC_a was generally smoother.

Figure 2d shows the 1mHcon collected on each of the three days. In general, average 1mHcon decreases with time. This is most likely due to the drying of the field. This was also evident in the range of the 1mHcon (Table 1), which decreased gradually from days 1 (52.6 mS m^{-1}), 4 (49.0) and 12 (43.7). Given this decrease was much larger than the systematic error caused by thermal expansion of the transmitter (<2 mS m^{-1}), we discount the effect of temperature. We believe this was the case because we conducted the DUALEM-421 survey at approximately the same time each day.

Distribution of soil properties along transect

Figure 3 shows contour plots of various soil properties. These figures were generated using the Contour Plot Tool available in JMP 10.2 (SAS 2012). Figure 3a shows clay with indicative soil texture. It is worth noting that the colors are plotted for clay content rather than soil

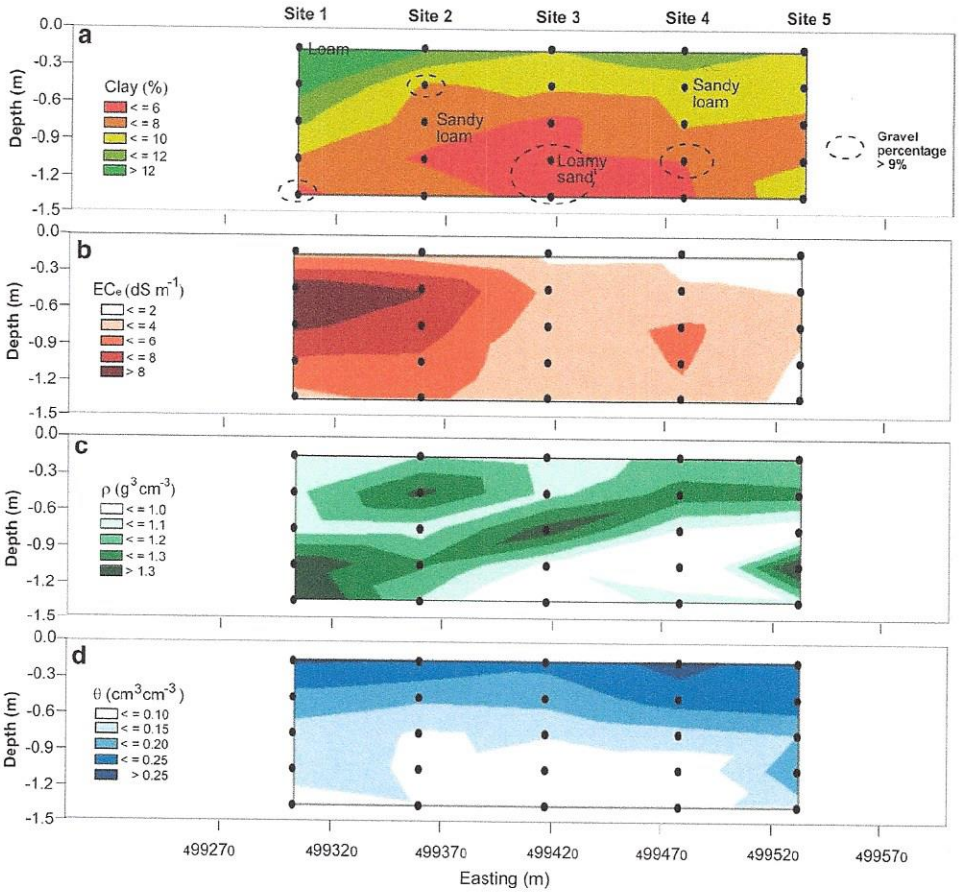

Fig. 3 Contour plots of various soil properties measured on day 1 at the 5 sampling sites and including **a** clay (%), **b** electrical conductivity of the saturation extract (EC_e, dS m^{-1}), **c** bulk density (ρ, g cm^{-3}) and **d** volumetric water content (θ, cm^3 cm^{-3}). *Note* Soil samples are marked in *black dots*. Samples with gravel percentage greater than 9 % were marked with *dash line circles* in **a**

texture. In general soil texture ranges from loam in the topsoil near the center pivot to sandy loams in the center, with subsoils of loamy sands. In the east soil texture is uniformly a sandy loam. We also note the high gravel (>9 %) in the subsurface (site 2), and subsoil (sites 3 and 4).

Figure 3b shows that in the eastern part of the field (site 5) EC_e measured from soil samples is non-saline (<2 dS m^{-1}) in the topsoil and deeper subsoil and slightly saline (2–4 dS m^{-1}) in the subsurface. At sites 3 and 4, EC_e is uniformly slightly saline. At sites 1 and 2, EC_e increases from non-saline to slightly saline and strongly saline (>8 dS m^{-1}) in the subsurface, before decreasing again gradually to non-saline levels.

Figure 3c shows ρ (g cm^{-3}) varies from small (0.9 g cm^{-3}) to moderate (1.4 g cm^{-3}). These values are consistent with previous results achieved by Corwin and Lesch (2013) across this field. Figure 3d shows volumetric water content (θ—cm^3 cm^{-3}) from day 1. In the topsoil θ is largest (>0.27 cm^3 cm^{-3}). Given the soil texture of the topsoil varies from Sandy Loams to Loams, this value of θ suggests the topsoil is saturated, given at field capacity θ for these textures ranges from 0.18–0.28 and 0.20–0.30 cm^3 cm^{-3}, respectively (Allen et al. 1998).

Conversely, the smallest θ (<0.10 cm^3 cm^{-3}) was in the center of the field (i.e., sites 2, 3 and 4). This value is equivalent to a value of θ at permanent wilting point for a loamy sand textured soil (Allen et al. 1998). This essentially represents θ prior to irrigation and in the subsoil. At a depth of approximately 0.75 m the intermediate-small θ (0.10–0.15 cm^3 cm^{-3}) therefore represents the wetting front.

Pearson's correlation coefficient between inverted σ and measured soil θ

Table 3 shows that the correlation between untransformed calculated true electrical conductivity (σ) with different soil properties (i.e., θ, clay, EC_e and ρ). It is evident that untransformed σ was most strongly correlated with θ on days 1 and 4 (Pearson's r = 0.79 and 0.61, respectively) and clay on the same 2 days (0.86 and 0.80, respectively). Untransformed σ was not strongly correlated with EC_e on days 1 and 4 (0.13 and 0.19, respectively), although on day 12 there was a small but significant correlation (0.42). There was no correlation between σ and ρ.

Figure 4a shows the calculated true electrical conductivity (σ) versus measured θ for different days. Different fitted lines are also highlighted. It is worth noting that the slope

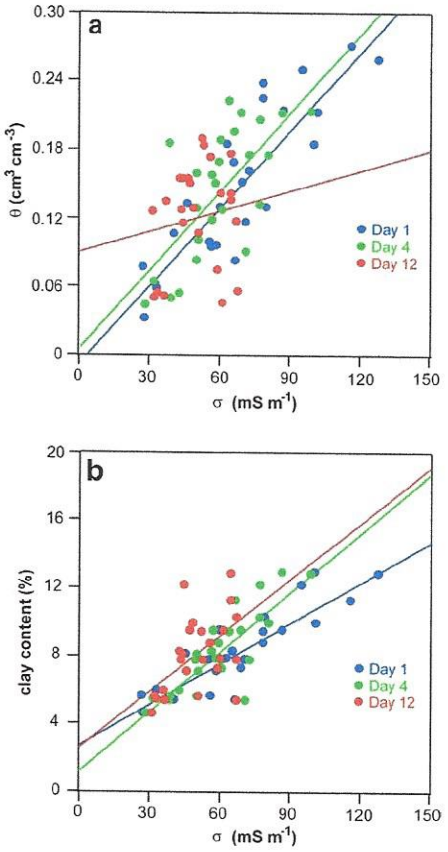

Fig. 4 **a** Soil volumetric water content (θ, $cm^3\ cm^{-3}$) and **b** clay content (%) collected on days 1, 4 and 12 versus corresponding calculated true electrical conductivity (σ, mS m^{-1}) generated using S2, FS, and λ of 0.6

of the line on days 1 and 4 are equivalent with only the intercept different. While the same cannot be said for the relationship for day 12, the fact that σ contracts in concert with a smaller range of θ indicates that most variation in σ can be explained by decrease in θ. Figure 4b shows σ versus clay for the different days. It shows that while the clay does not change, σ decreases as soil θ decreases.

Spatio-temporal distribution of soil σ along the study transect on different days

Figure 5 shows the contour plot of calculated true electrical conductivity (σ) across the transect on different days. Figure 5a shows σ on day 1. It is apparent σ is large (>100 mS m^{-1}) in close proximity to site 1 and in the topsoil (0–0.3 m) and subsurface (0.3–0.6 m). Along the rest of the transect σ in the topsoil decreases to intermediate-large (85–100 mS m^{-1}) while subsurface σ also decreases to intermediate values (70–85 mS m^{-1}).

In most places subsoil σ is either intermediate-small (55–70 mS m^{-1}) or small (<55 mS m^{-1}). Particularly, in the center of the field, subsoil σ is uniformly small (<55 mS m^{-1}). This is consistent with the measured soil θ which shows that these profiles may be close to the permanent wilting point. Conversely, it is worth noting the lack of subsurface σ (<40 mS m^{-1}) in some locations. This is the case to the east of site 3 (Easting 499,440 m). This is because this profile is situated directly beneath a tire track of the A-frame gantry.

Here the soil is most likely compacted and the higher ρ inhibits water infiltration. Michot et al. (2003) described the same phenomenon when monitoring changes in water content using electrical resistivity tomography. Figure 5b, c shows σ on day 4 and day 12, respectively. The spatial patterns are equivalent to day 1, albeit the soil appears to becoming less conductive with time.

Percentage contribution of total variance of MRA components

In order to understand the scale-specific spatio-temporal variation in soil σ with depth over 12 days, we calculated the two-dimensional MRA components of the EMCI. Table 2 shows the percent contribution of total variance in σ by MRA detailed horizontal components (LH1–LH6) and smooth components at the coarsest scale (LL6).

On day 1 we found that the dominant scales of variation in σ occur at 9.3–18.7 (50.21 %), >74.7 (23.18 %) and 4.7–9.3 m (16.29 %). This is consistent with Lark et al. (2003), who used one-dimensional MRA to understand the EC_a variation in a 32.4-ha salt-affected site primarily dominated with Lethent clay loam. Conversely, the smallest percentage of variation was LH6 (0.35 %) and LH5 (0.67 %). This indicates variation in σ is not important at spatial scales of 37.3–74.7 or 18.7–37.3 m, respectively. The same can be said about LH2 (3.38 %) and LH1 (5.93 %) which although accounting for 5–10 times as much variation is still small compared with components LH3 (16.29 %), LL6 (23.18 %) and LH4 (50.21 %), which were more than 25 times larger.

The meaning of these results is that the horizontal variation of the EMCIs was mostly within intermediate and large spatial scales and occurs at distances of 9.3–18.7 m (LH4), >74.7 m (LL6) and 4.7–9.3 m (LH3). We note that some variation in σ may occur at spatial scales other than the ones mentioned. This is because MRA can only extract the variations within predefined scale intervals and fails to accounts for the variations within other possible scale intervals (Biswas et al. 2013).

Scale-specific correlations between 2-d MRA of σ and soil properties

In order to understand the results shown in Table 3 we correlate the MRA components with the various soil properties

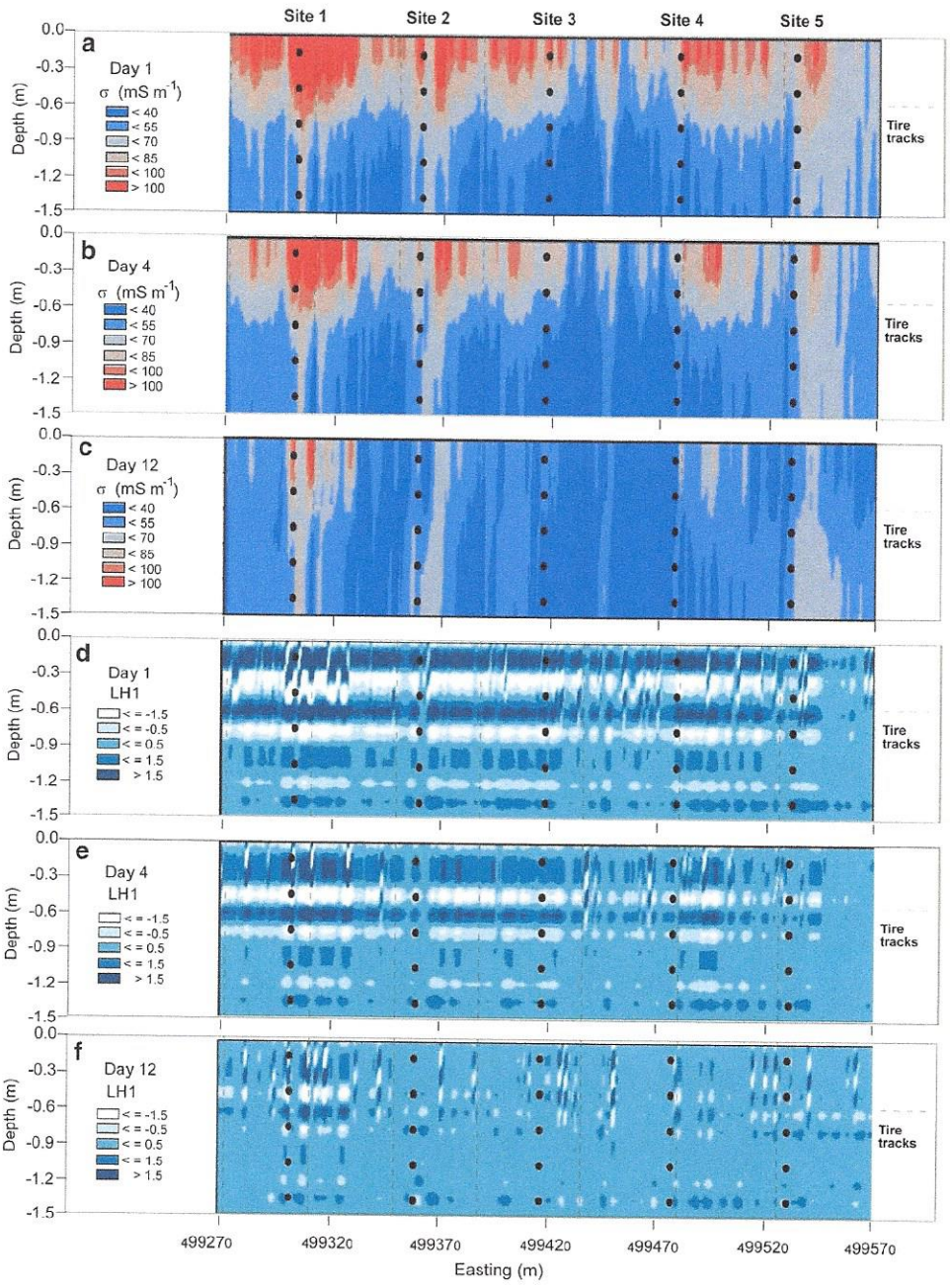

Fig. 5 Spatial distribution of calculated true electrical conductivity (σ, mS m^{-1}) generated using S2, FS, and λ of 0.6 on days **a** 1, **b** 4 and **c** 12, and multi-resolution analysis (MRA) component LH1(1.2–2.3 m) of these σ on days **d** 1, **e** 4 and **f** 12, respectively. *Note* Soil samples are marked in *black dots*

which influence σ, namely θ, clay, EC_e and ρ. Table 3 shows the Pearson's correlation coefficients (r) between 2-d MRA detailed components in the horizontal direction (LH1–6) and the smooth component (LL6) at the coarsest scale with different soil properties. In describing the results we point out that the correlation between the 2-d MRA σ and θ occurs on samples taken every day (i.e., days 1, 4 and 12), whereas the correlation between 2-d MRA and the other soil properties occurs only on the soil data collected on day 1. This is because we assume these soil properties do not change and we only measured these on day 1.

Table 3a shows the correlation with θ on day 1. The first point to make is that θ was best correlated with LH5 (Pearson's $r = 0.86$, $P < 0.001$), LH6 (0.84) and LH4 (0.83), surpassing the correlation with σ (0.79). This indicates that to estimate θ across this transect we would be best served using any of these components as a covariate than σ. The reason for the strong correlations at these scales (i.e., 18.7–37.3, 37.3–74.7 and 9.3–18.7 m) would appear to be a function of various aspects of the pivot system and agronomy. With respect to 37.3–74.7 m scale, this would appear to be a function of the spacing of the

Table 2 Percent contribution of total variance in calculated true electrical conductivity (σ) by multi-resolution analysis (MRA) detailed horizontal components (LH1–LH6) and smooth components at the coarsest scale (LL6)

MRA components	Day 1 (%)	Day 4 (%)	Day 12 (%)
LH1 (1.2–2.3 m)	5.93	5.29	6.69
LH2 (2.3–4.7 m)	3.38	3.38	3.00
LH3 (4.7–9.3 m)	16.29	15.13	10.22
LH4 (9.3–18.7 m)	50.21	45.90	30.21
LH5 (18.7–37.3 m)	0.67	0.61	0.38
LH6 (37.3–74.7 m)	0.35	0.31	0.18
LL6 (>74.7 m)	23.18	29.38	49.32

A-frame of the pivot gantry, which has an average spacing of 48 m.

It is not clear what the scale of 18.7–37.3 m represents, however, and based on observations from Google Earth imagery (06/08/2012) and local knowledge from the farmers, it appears that the turning circle of the tractor necessitates passes to cut the alfalfa which are 16, 24 or 32 m apart. At the smaller spatial scale of 9.3–18.7 m, this is a most likely a function of the spacing between passes of the alfalfa cutter given its width is 8 m. At both these scales, the increased soil ρ in the cutter tire tracks appears to be influencing θ.

Table 3b shows the correlation between the MRA components with clay. It is necessary to point out that clay was best correlated with untransformed σ on day 1 (Pearson's $r = 0.86$, $P < 0.001$). As with θ the best correlation between wavelet transformed σ and clay was LH4 (0.80) followed by LH5 and LH6 (0.79). This indicates that at spatial scales of 9.3–18.7, 18.7–37.3 and 37.3–74.7 m, clay controls σ in spite of the fact that clay is small and is not very variable as indicated in Fig. 3a (i.e., ~6–12 %). Equivalent results can be seen on day 4 and day 12; however, the correlations diminish and in line with decreasing θ (see Table 3b).

Interestingly, and at the smallest scale (i.e., LH1), clay is not correlated with σ on day 1 (0.31) but it is on day 4 (−0.52) and 12 (−0.59). This is most likely because on day 1, the soil is uniformly wet and the clay does not affect the distribution of σ at the smallest scale (1.2–2.3 m) but on days 4 and 12, the contribution of clay to σ increases as the soil dries. It is also worth noting that regardless of the day after irrigation, the largest scale LL6 remains constant (0.41), which indicates that the trend in decreasing clay away from the center pivot (see Fig. 3a) influences σ on all days. Table 3c shows the correlation with soil EC_e.

We reiterate that EC_e is not correlated with untransformed σ (e.g., day 1, $r = 0.13$). However, as with clay, it is correlated with LL6 on days 1 (0.49), 4 (0.47) and 12 (0.38). This suggests at a scale of >74.7 m, EC_e (see Fig. 3b) has some effect on σ. In this case, it is a function of the decreasing salinity from west to east. Specifically, the decreasing trend from near the center pivot where EC_e is moderately saline (8–12 dS m^{-1}) to where it is non-saline (<2 dS m^{-1}) furthest from the center. The implication for

Table 3 Pearson's correlation (r) coefficients between two-dimensional multi-resolution analysis (MRA) detailed components in the horizontal direction (LH1–LH6) and the smooth component (LL6) at the coarsest scale of the calculated true electrical conductivity (σ) with the corresponding measured soil properties, including (a) volumetric water content (θ), (b) clay content, (c) electrical conductivity of the saturated soil-paste extract (EC_e) and (d) bulk density (ρ)

MRA component	Day 1	Day 4	Day 12
(a)			
LH1 (1.2–2.3 m)	0.40*	−0.41*	−0.32
LH2 (2.3–4.7 m)	0.11	−0.01	−0.29
LH3 (4.7–9.3 m)	0.54**	0.28	0.01
LH4 (9.3–18.7 m)	0.83***	0.67***	0.26
LH5 (18.7–37.3 m)	0.86***	0.70***	0.22
LH6 (37.3–74.7 m)	0.84***	0.72***	0.25
LL6 (>74.7 m)	0.16	0.30	0.06
Untransformed σ	0.79***	0.61**	0.01
(b)			
LH1 (1.2–2.3 m)	0.31	−0.52**	−0.59**
LH2 (2.3–4.7 m)	−0.02	0.07	−0.20
LH3 (4.7–9.3 m)	0.39	0.39	0.08
LH4 (9.3–18.7 m)	0.80***	0.77***	0.35
LH5 (18.7–37.3 m)	0.79***	0.79***	0.35
LH6 (37.3–74.7 m)	0.79***	0.80***	0.50*
LL6 (> 74.7 m)	0.41*	0.41*	0.41*
Untransformed σ	0.86***	0.80***	0.42*
(c)			
LH1 (1.2–2.3 m)	−0.49*	−0.54**	−0.32
LH2 (2.3–4.7 m)	−0.54**	−0.55**	−0.38
LH3 (4.7–9.3 m)	−0.51**	−0.49*	−0.48*
LH4 (9.3–18.7 m)	0.04	0.06	0.05
LH5 (18.7–37.3 m)	−0.04	−0.03	0.01
LH6 (37.3–74.7 m)	0.04	0.04	0.05
LL6 (>74.7 m)	0.49*	0.47*	0.38
Untransformed σ	0.13	0.19	0.42*
(d)			
LH1 (1.2–2.3 m)	−0.09	0.03	0.02
LH2 (2.3–4.7 m)	0.02	−0.01	−0.04
LH3 (4.7–9.3 m)	−0.02	−0.07	0.08
LH4 (9.3–18.7 m)	−0.08	−0.13	−0.17
LH5 (18.7–37.3 m)	−0.08	−0.11	−0.21
LH6 (37.3–74.7 m)	-0.08	−0.09	−0.22
LL6 (>74.7 m)	0.32	0.32	0.32
Untransformed σ	0.08	0.00	0.25

* $P < 0.05$; ** $P < 0.01$; *** $P < 0.001$

salinity management is more water could be applied close to the center pivot to increase leaching fraction, thereby removing salts applied to the loamy soil.

In addition, LH3 (4.7–9.3 m) is correlated with EC_e on days 1 (−0.51), 4 (−0.49) and 12 (−0.48), with strong correlations with LH1 (1.2–2.3 m) and LH2 (2.3–4.7 m) on the first 2 days. These results suggest that if we wanted to map EC_e across this transect we are best served using the correlation between LH1, LH2 or LH3 and EC_e rather than with σ. The result in terms of irrigation management is also potentially informative, because the correlation between EC_e and LH1 is consistent with the average spacing of the sprinklers (i.e., 1.2 and 1.6 m). However, it is not immediately apparent what the significance of this result means.

Table 3d shows the correlation with soil ρ. It is found that neither σ nor 2-d MRA components are significantly correlated with soil σ. This is most likely a function of the fact that we did not collect enough soil samples at a small enough scale and more particularly at the locations where ρ is significant. That is beneath the tire tracks of the alfalfa cutter or the A-frame of the center pivot gantry.

Spatial distributions of two-dimensional horizontal MRA components on different days

To better understand the scale-specific spatio-temporal variation in θ with depth on different days, we plotted the spatial distributions of 2-d MRA components in Figs. 5d–f, 6 and 7. It is worth pointing out that the change in the 2-d MRA components over small distances, either vertical and/or horizontal, is more important than whether the components are large or small. For example, and as shown in Fig. 5d which shows component LH1 on day 1, the greatest changes vertically occur at depths of around 0.1, 0.2, 0.5 and 0.7 m. These changes would appear to be some function of various soil water interactions and including areas of saturated flow, change in soil texture and the wetting front.

We also note the distribution of LH1 in the topsoil and upper subsurface is uneven and shows periodically large (>1.5) and small (<−1.5) values in the horizontal direction which occur in places and at an approximate spacing of 6–10 m. This is particularly the case between site 3 and site 4. From a Google image (06/08/2012), we have identified that this periodic change coincides with the location of the tire tracks associated with the alfalfa cutter. This suggests that ρ in these tire tracks influences σ and therefore θ given the strong correlation shown between them in Table 3a.

Figure 5e shows that the short-scale variation in σ is similar vertically and in the topsoil (0–0.3 m) and subsurface (0.3–0.6 m). This may imply there is not much vertical variation in θ from day 1 to day 4 at these depths as the soil has not dried out. However, there is less variation horizontally and in the subsoil (0.6–0.9 m). This becomes increasingly more apparent on day 12 and as shown in Fig. 5f and at subsoil depths. At this depth it is evident that the LH1 is mostly intermediate (−0.5 to 0.5). This indicates several soil properties are changing subtly at this small scale. However, the remaining variation in σ in the horizontal direction is most likely due to compaction caused by the cutter tire tracks.

Figure 6a shows LH3 on day 1 and indicates where σ variation occurs at a scale of 4.7–9.3 m. Firstly, it is worth noting that a change of LH3 occurs between the largest LH3 values (>3) which characterize the topsoil (0–0.3 m) and the smallest LH3 (<−3) which defines the subsurface (0.3–0.6 m) and subsoil (0.6–1.2 m). This depth interval is consistent with the approximate depth where topsoil pore space in the loam and sandy loams would appear to be near saturation on day 1 and as inferred from Fig. 3d. This also indicates that at least in terms of irrigation efficiency the pivot irrigation system is supplying uniform application of water along the entire transect.

Of equal importance is the variation in LH3 in the horizontal direction. Figure 6a, b shows that on day 1 and day 4 there is not much variation in the topsoil and/or the subsurface along the transect. However, it is evident on day 4 (Fig. 6b) and on day 12 (Fig. 6c) that there is substantially more variation. This indicates that several soil properties are changing within this scale (i.e., 4.7–9.3 m) but most likely as a result of the removal of θ through evapotranspiration and/or deep drainage. It is also as a function of the coarser nature of soil texture and more significantly the gravel percentage which was much larger (>9 %) at various depths at these sites and as indicated in Fig. 3a.

Figure 6d, e shows the distributions of LH4 on days 1 and 4, respectively. Unlike the vertical variations in LH1 and LH3, there is no abrupt change in LH4 in this direction. Similar variation is also evident in Fig. 7a, b which shows the distributions of LH6 on days 1 and 4, respectively. The most important observation to make here is that the change in LH4 and LH6 occurs at a depth interval of 0.6–0.9 m. This depth interval is consistent with the approximate depth at which we suspect the wetting front of the irrigated water is most likely to be found and is consistent with the average intermediate-small θ (0.10–0.15 cm^3 cm^{-3}) and shown in Fig. 3d.

Figure 7d–f shows the distribution of LL6 on days 1, 4 and 12, respectively. As Lark and Webster (2004) and Biswas et al. (2013) suggest, the smooth MRA component represents the overall trend of the target soil property across a study area. Given the correlation between LL6 with clay and EC_e (Table 3b, c, respectively), we conclude that variation in σ at this scale (>74.7 m) was a function of the decreasing clay and EC_e across the transect and from west to east.

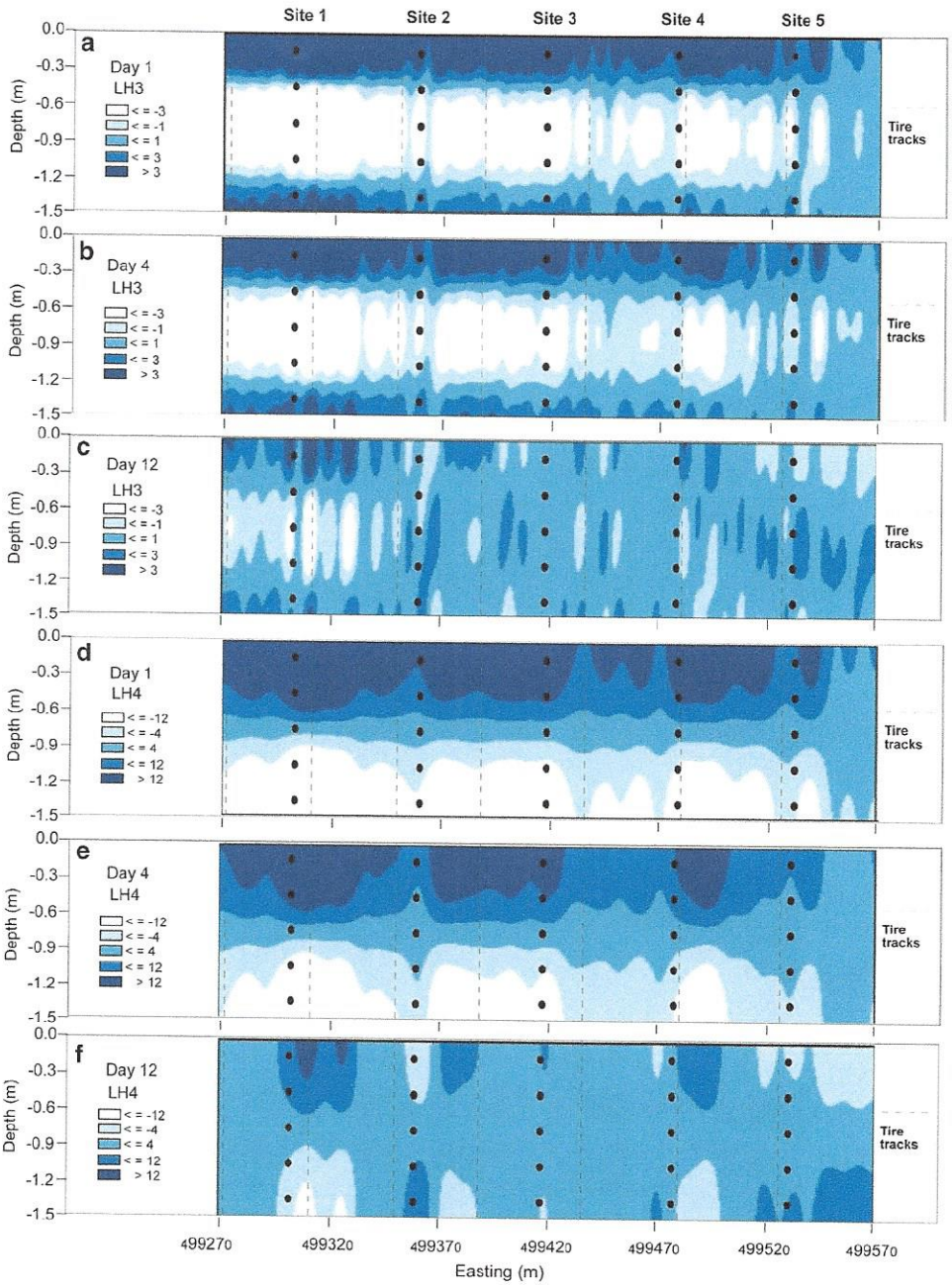

Fig. 6 Spatial distribution of multi-resolution analysis (MRA) components of calculated true electrical conductivity (σ, mS m^{-1}), including LH3 (4.7–9.3 m) on days **a** 1, **b** 4 and **c** 12 and LH4 (9.3–18.7 m) on days d) 1, **e** 4 and **f** 12, respectively. *Note* Soil samples are marked in *black dots*

Conclusions

The study shows how inversion of EC_a data and the examination of the EMCI along a 350-m transect on different days can be interpreted with reference to various soil properties which are influencing σ. We conclude that σ is most strongly correlated with θ and clay. Further, and by using a two-dimensional multi-resolution analysis (MRA), we characterized the spatio-temporal variation in σ. The dominant scales of variation in σ occur at 9.3–18.7 (50.21 %), >74.7 (23.18 %) and 4.7–9.3 m (16.29 %). We conclude the variation between distance interval 9.3–18.7 and 4.7–9.3 m may be a function of the width of the alfalfa cutter (8 m), while >74.7 m we attribute to the clay and salinity and to a lesser extent the tire track spacing of the irrigation gantry (~48 m). The spacing in sprinklers (1.2 and 1.6 m) explains the minor variation at the short spatial scale of 1.2–2.3 m (5.93 %). In order to better account for the influence of θ and salinity on σ at certain scales and with time, future work should look at the use of sensors which can measure these properties continuously.

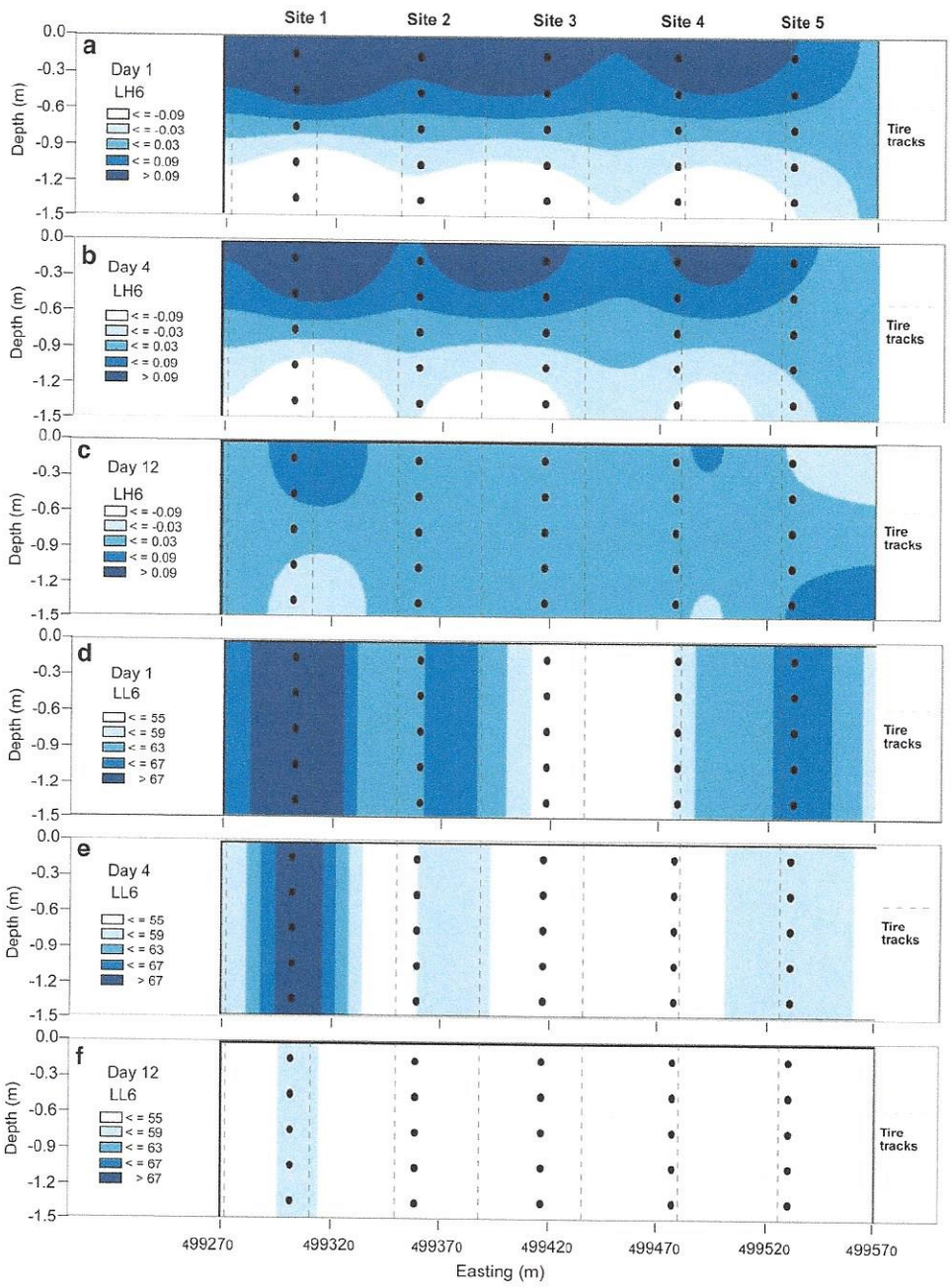

Fig. 7 Spatial distribution of multi-resolution analysis (MRA) components of calculated true electrical conductivity (σ, mS m^{-1}), including LH6 (37.3–74.7 m) on days **a** 1, **b** 4 and **c** 12 and LL6 (>74.7 m) on days **d** 1, **e** 4 and **f** 12, respectively. *Note* Soil samples are marked in *black dots*

In addition, by correlating the MRA components with the various soil properties, several management implications can be concluded. Firstly, at the short (1.2–2.3 m) spatial scale (LH1) the periodic change in the horizontal direction (6–8 m) coincides with the location of the tire tracks of the alfalfa cutter and indicates the ρ in these tire tracks influences θ. The implication is that these areas need to be ameliorated to increase productivity. At larger spatial scales (4.7–9.3 m) change in LH3 mainly occurs vertically between topsoil and subsurface, which was consistent with the approximate depth (0.3 m) of saturation. This indicates that in terms of irrigation efficiency the pivot irrigation system is supplying uniform water along the entire transect. Thirdly, the change in LH4 (9.3–18.7 m) and LH6 (37.3–74.7 m) occur at a deeper depth interval (0.6–0.9 m) which is consistent with the approximate depth of the wetting front. Lastly, at the larger spatial scale (LL6: >74.7 m) the variation is attributable to the generally decreasing clay and EC_e across the transect from west to east. The management implication here is that the rate of irrigation may need to be increased closer to the center pivot to increase the leaching fraction and removal of salts.

Acknowledgments The authors acknowledge the numerous hours of diligent technical work performed in the field and the laboratory by Kevin Yemoto and Wes Clary. We thank Scott's Brothers Dairy Farm, particularly Bruce Scott, for allowing unrestricted access to their property and allowing us to undertake the research.

References

Abdu H, Robinson DA, Seyfried M, Jones SB (2008) Geophysical imaging of watershed subsurface patterns and prediction of soil texture and water holding capacity. Water Resour Res. doi:10.1029/2008WR007043

Akbar MA, Kenimer AL, Searcy SW, Torbert HA (2005) Soil water estimation using electromagnetic induction. T ASAE 48(1):129–135

Allen RG, Pereira LS, Raes D, Smith M (1998) Crop evapotranspiration. FAO irrigation and Drainage Paper 56, Food and Agriculture Organization of the United Nations, Rome, p 144

Auken E, Foged N, Sorensen KI (2002) Model recognition by 1-D laterally constrained inversion of resistivity data. In: Matias MS, Grangeia C (eds) Proceedings of 8th meeting environmental and engineering geophysics, EEGS-ES. University of Aveiro, Portugal, pp 241–244

Biswas A, Si BC, Walley FL (2008) Spatial relationship between δ15N and elevation in agricultural landscapes. Nonlinear Proc Geoph 15(3):397–407. doi:10.5194/npg-15-397-2008

Biswas A, Cresswell HP, Chau HW, Viscarra Rossel RA, Si BC (2013) Separating scale-specific soil spatial variability: a comparison of multi-resolution analysis and empirical mode decomposition. Geoderma 209:57–64. doi:10.1016/j.geoderma.2013.06.003

Brevik EC, Fenton TE, Lazari A (2006) Soil electrical conductivity as a function of soil water content and implications for soil mapping. Precis Agric 7(6):393–404. doi:10.1007/s11119-006-9021-x

Corwin DL, Lesch SM (2013) Protocols and guidelines for field-scale measurement of soil salinity distribution with ECa-directed soil sampling. J Environ Eng Geophys 18(1):1–25. doi:10.2113/JEEG18.1.1

Corwin DL, Kaffka SR, Hopmans JW, Mori Y, Van Groenigen JW, Van Kessel C, Lesch SM, Oster JD (2003) Assessment and field-scale mapping of soil quality properties of a saline-sodic soil. Geoderma 114(3):231–259. doi:10.1016/S0016-7061(03)00043-0

Corwin DL, Hopmans J, de Rooij GH (2006) From field- to landscape-scale vadose zone processes: scale issues, modeling, and monitoring. Vadose Zone J 5(1):129–139. doi:10.2136/vzj2006.0004

Corwin DL, Lesch SM, Segal E, Skaggs TH, Bradford SA (2010) Comparison of sampling strategies for characterizing spatial variability with apparent soil electrical conductivity directed soil sampling. J Environ Eng Geophys 15(3):147–162. doi:10.2113/JEEG18.1.1

Daubechies I (1992) Ten lectures on wavelets, vol. 61 of CBMS-NSF Regional Conference Series in Applied Mathematics

EMTOMO (2014) EM4Soil Version 2. EMTOMO, R. Alice Cruz 4, Odivelas, Lisboa, Portugal

Friedman SP (2005) Soil properties influencing apparent electrical conductivity: a review. Comput Electron Agric 46(1):45–70. doi:10.1016/j.compag.2004.11.001

Goff A, Huang J, Wong VNL, Monteiro Santos FA, Wege R, Triantafilis J (2014) Electromagnetic conductivity imaging of soil salinity in an estuarine–alluvial landscape. Soil Sci Soc Am J 78(5):1686–1693. doi:10.2136/sssaj2014.02.0078

Gómez-Plaza A, Alvarez-Rogel J, Albaladejo J, Castillo VM (2000) Spatial patterns and temporal stability of soil moisture across a range of scales in a semi-arid environment. Hydrol Process 14(7):1261–1277

Grinsted A, Moore JC, Jevrejeva S (2004) Application of the cross wavelet transform and wavelet coherence to geophysical time series. Nonlinear Proc Geophys 11(5/6):561–566

Huang J, Davies GB, Bowd D, Monteiro Santos FA, Triantafilis J (2014) Spatial prediction of the exchangeable sodium percentage at multiple depths using electromagnetic inversion modelling. Soil Use Manage 30(2):241–250. doi:10.1111/sum.12106

Huang J, Shi Z, Biswas A (2015) Characterizing anisotropic scale-specific variations in soil salinity from a reclaimed marshland in China. Catena 131:64–73. doi:10.1016/j.catena.2015.03.011

Huang J, Scudiero E, Choo H, Corwin DL, Triantafilis J (2016a) Mapping soil moisture across an irrigated field using electromagnetic conductivity imaging. Agric Water Manage 163:285–294. doi:10.1016/j.agwat.2015.09.003

Huang J, Scudiero E, Clary W, Corwin DL, Triantafilis J (2016b) Time-lapse monitoring of soil water content using electromagnetic conductivity imaging. Soil Use Manage. doi:10.1111/sum.12261

Kachanoski RG, Wesenbeeck IV, Gregorich E (1988) Estimating spatial variations of soil water content using noncontacting electromagnetic inductive methods. Can J Soil Sci 68(4):715–722. doi:10.4141/cjss88-069

Kachanoski RG, Wesenbeeck IV, Jong ED (1990) Field scale patterns of soil water storage from non-contacting measurements of bulk electrical conductivity. Can J Soil Sci 70(3):537–542. doi:10.4141/cjss90-056

Knox JW, Kay MG, Weatherhead EK (2012) Water regulation, crop production, and agricultural water management—understanding farmer perspectives on irrigation efficiency. Agric Water Manage 108:3–8. doi:10.1016/j.agwat.2011.06.007

Lark RM, Webster R (1999) Analysis and elucidation of soil variation using wavelets. Eur J Soil Sci 50(2):185–206. doi:10.1046/j.1365-2389.1999.t01-1-00234.x

Lark RM, Webster R (2004) Analysing soil variation in two dimensions with the discrete wavelet transform. Eur J Soil Sci 55(4):777–797. doi:10.1111/j.1365-2389.2004.00630.x

Lark RM, Kaffka SR, Corwin DL (2003) Multiresolution analysis of data on electrical conductivity of soil using wavelets. J Hydrol 272(1):276–290. doi:10.1016/S0022-1694(02)00271-8

Lark RM, Milne AE, Addiscott TM, Goulding KWT, Webster R, O'Flaherty S (2004) Scale- and location-dependent correlation of nitrous oxide emissions with soil properties: an analysis using wavelets. Eur J Soil Sci 55(3):611–627. doi:10.1111/j.1365-2389.2004.00620.x

Li HY, Shi Z, Webster R, Triantafilis J (2013) Mapping the three-dimensional variation of soil salinity in a rice–paddy soil. Geoderma 195:31–41. doi:10.1016/j.geoderma.2012.11.005

Mallat SG (1989) A theory for multiresolution signal decomposition: the wavelet representation. IEEE Trans Pattern Anal Mach Intell 11(7):674–693. doi:10.1109/34.192463

Mallat SG (1999) A wavelet tour of signal processing. Academic Press, New York

McBratney AB (1998) Some considerations on methods for spatially aggregating and disaggregating soil information. Nutr Cycl Agroecosyst 50:51–62. doi:10.1007/978-94-017-3021-1_5

Michot D, Benderitter Y, Dorigny A, Nicoullaud B, King D, Tabbagh A (2003) Spatial and temporal monitoring of soil water content with an irrigated corn crop cover using surface electrical resistivity tomography. Water Resour Res 39(5):1138. doi:10.1029/2002WR001581

Pebesma EJ (2004) Multivariable geostatistics in S: the gstat package. Comput Geosci 30(7):683–691. doi:10.1016/j.cageo.2004.03.012

Percival DB, Walden AT (2000) Wavelet methods for time series analysis. Cambridge University Press, New York

Rhoades JD, Kandiah A, Mashali AM (1992) The use of saline waters for crop production. FAO irrigation and drainage paper, no. 48, pp 133

SAS Institute (2012) JMP version 10. SAS Institute Inc., Cary

Sheets KR, Hendrickx JM (1995) Noninvasive soil water content measurement using electromagnetic induction. Water Resour Res 31(10):2401–2409. doi:10.1029/95WR01949

Sherlock MD, McDonnell JJ (2003) A new tool for hillslope hydrologists: spatially distributed groundwater level and soil water content measured using electromagnetic induction. Hydrol Process 17(10):1965–1977. doi:10.1002/hyp.1221

US Salinity Laboratory Staff (1954) Diagnosis and improvement of saline and alkali soils. USDA Handbook 60, U.S. Government Printing Office, Washington, DC

Triantafilis J, Monteiro Santos FA (2009) 2-dimensional soil and vadose zone representation using an EM38 and EM34 and a laterally constrained inversion model. Aust J Soil Res 47(8):809–820. doi:10.1071/SR09013

Triantafilis J, Monteiro Santos FA (2013) Electromagnetic conductivity imaging (EMCI) of soil using a DUALEM-421 and inversion modelling software (EM4Soil). Geoderma 211–212:28–38. doi:10.1016/j.geoderma.2013.06.001

Triantafilis J, Terhune CH IV, Monteiro Santos FA (2013) An inversion approach to generate electromagnetic conductivity images from signal data. Environ Model Software 43:88–95. doi:10.1016/j.envsoft.2013.01.012

Vanwalleghem T, Stockmann U, Minasny B, McBratney AB (2013) A quantitative model for integrating landscape evolution and soil formation. J Geophys Res Earth Surf 118(2):331–347

Vörösmarty CJ, Green P, Salisbury J, Lammers RB (2000) Global water resources: vulnerability from climate change and population growth. Science 289(5477):284–288. doi:10.1029/2011JF002296

Whitcher B (2015) Basic wavelet routines for one-, two- and three-dimensional signal processing. R Package 'waveslim', version 1.7.5., published online on 2015/01/10

Zare E, Huang J, Monteiro Santos FA, Triantafilis J (2015) Mapping salinity in three-dimensions using a DUALEM-421 and electromagnetic inversion software. Soil Sci Soc Am J 79:1729–1740. doi:10.2136/sssaj2015.06.0238